1Pa-54

Proceedings of Symposium on Ultrasonic Electronics, Vol. 31 (2010) pp. 123-124
6-8 December, 2010

Multi-element diverging beam from a Linear Array Transducer for transverse cross-sectional imaging of Carotid Artery

Akinlolu PONNLE[1†], Hideyuki HASEGAWA[2,1] and Hiroshi KANAI[1,2]
([1]Grad. School of Eng., Tohoku Univ.; [2]Grad. School of Biomed. Eng., Tohoku Univ.)

1. Introduction

Transverse cross-sectional ultrasound imaging of the intima-media complex of the carotid arterial wall is difficult to obtain using conventional linear scanning because focused ultrasound beams are perpendicular to the wall in a limited region. This makes the angular width of the imaged region of the anterior and posterior walls, subtended at the center of cross-section of the artery to be limited.

Previous attempts to increase the angular width generally involves steering of focused transmit beams as used in spatial multi-angle compound imaging (MACI) [1], or specifically designing each scan beam to pass through the center of the artery over a limited region [2] or perpendicular to vascular walls at predetermined positions along the wall [3]. However, transmit steering angle is limited because of increase in amplitude of grating lobes with steering. Also, in some cases, combination of multiple frames reduces overall compound frame rate as well as producing temporal compounding in real time applications.

By using diverging beam from a linear array transducer, a wider angular width of imaged region could be obtained (which can increase with number of transmissions) without steering of transmit beams at the same frame rate as of conventional linear scanning. Also, receive grating lobe problem can be reduced (with improved resolution) by focusing from multiple transmissions. This type of beam has previously been investigated for various purposes by Karaman *et al.* [4], Lockwood *et al.* [5] and Nikolov *et al.* [6].

In this study, this beam was investigated for transverse cross-sectional imaging of cylindrical vessels and images were reconstructed by multi-angle receive steering and focusing from multiple transmissions. Acoustic field simulation and measurement, virtual scanning of a simulated reflector-tube and scanning of a silicone-rubber tube phantom in water were performed. An illustration of this beam is shown in **Fig. 1**(a).

2. Principle

2.1 Transmit beam-forming

In multi-element diverging beam production, the excitation of each of the sub-aperture elements is time-delayed in such a way that spherical resultant wavefronts diverges in front of the transducer array over a limited angle as illustrated in Fig. 1(b).

E-mail: ponnle@us.ecei.tohoku.ac.jp
{hasegawa, kanai}@ecei.tohoku.ac.jp

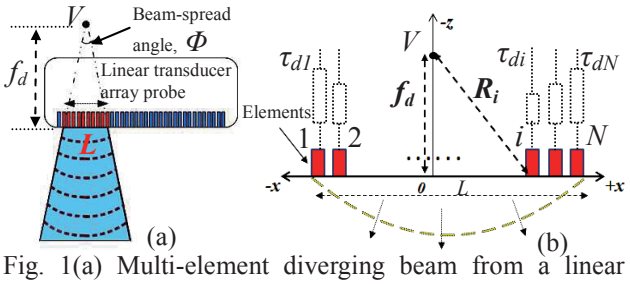

Fig. 1(a) Multi-element diverging beam from a linear array transducer. V is the virtual acoustic source behind the array surface and f_d is the axial distance of the virtual acoustic source from the array surface. (b) Time-delay for each element in the sub-aperture.

The delay, τ_{di}, for an element i (i = 1, 2, 3, … N) is calculated by

$$\tau_{di} = \frac{R_i - f_d}{c}, \tag{1}$$

where R_i is the distance of center of element i from the virtual acoustic source V, and c is the speed of sound in the medium.

In transmission, active sub-apertures are stepped across the array at a lateral pitch of one-element with coincident transmit and receive sub-apertures.

2.2 Receive

For an image point $\boldsymbol{p}$ at position (x_p,z_p), the receiving beam is steered by the sub-aperture through angle θ_{rs} to receive-focus on $\boldsymbol{p}$ (**Fig. 2**).

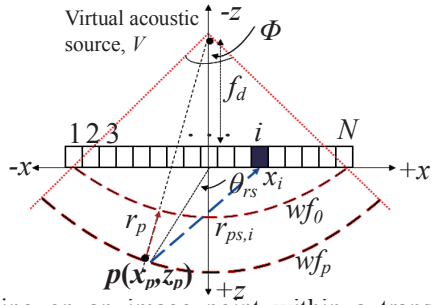

Fig. 2 Focusing on an image point within a transmit beam.

If $y_{nt,i}(t)$ represents the received echo signal on element i for the nt-th transmission, final beamformed image at $\boldsymbol{p}$, S_p, is expressed as

$$S_p = \sum_{nt=1}^{N_T} \sum_{i=1}^{N} w_i y_{nt,i}(t_p), \tag{2}$$

where w_i is the apodization weight for element i and N_T is the number of transmissions that point $\boldsymbol{p}$ lies within their transmit beams. t_p is the time of flight of ultrasound from the beginning of reception to reach receive element, i via point $\boldsymbol{p}$ and is given as

$$t_p = \frac{r_p + r_{ps,i}}{c}, \tag{3}$$

where r_p is the distance covered by the transmit wavefront from received time $t = 0$ to the image point, as shown in Fig. 2 and $r_{ps,i}$ is the distance covered by scattered signal from the image point to receive element, i.

3. Acoustic field - simulations and measurement

The acoustic field of the diverging beam was simulated using Field II program [7]. The excitation was set at a frequency of 10 MHz, and active transmit sub-aperture of 96 elements with virtual acoustic source distance, f_d = 10 mm behind the array surface. Also, acoustic field measurement in water was performed using a hydrophone, α-10 ALOKA ultrasound machine and a linear array transducer with the same transmit parameters as used in the simulation.

Figures 3(a) and (b) show the simulated pressure waves and RF signals from the hydrophone respectively at depths of 10 mm and 20 mm below the transducer surface. Diverging (spherical) wavefronts was achieved in this range which corresponds to the typical depth of carotid artery below the skin surface.

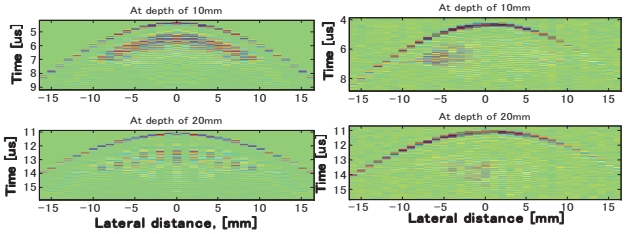

(a) (b)

Fig. 3 Simulated emitted waves (a) and RF signals from the hydrophone (b) at depths of 10 mm and 20 mm.

4. Virtual scanning and phantom scanning

Transverse cross-sectional view of a 'tube-shaped' reflector composed of point-scatterers of equal strength and inter-scatterer spacing of 20 μm in water was simulated and a virtual scanning was performed using Field II program [7].

Also, transverse cross-sectional scanning of a silicone-rubber tube phantom in water was performed using α-10 ALOKA ultrasound machine and a linear array transducer probe. Two separate scans were performed (focused beams and spherical beams, both at a frame rate of 110 Hz). Ultrasonic RF echoes were received at a center frequency of 10 MHz and sampled at a frequency of 40 MHz.

5. Results

Figures 4 and 5 show the reconstructed images obtained from simulated scanning of the simulated 'tube-reflector' and silicone rubber-tube phantom scanning, respectively for various numbers of consecutive sequential transmissions. The angular width of the imaged region of the tube's wall is wider than that in the conventional focused beam image. Wider angle is obtained for 95 transmissions than for 29 transmissions.

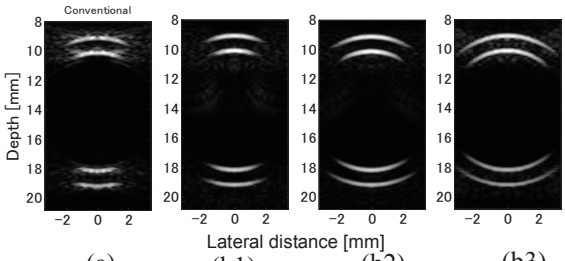

(a) (b1) (b2) (b3)

Fig. 4 Reconstructed B-mode images of the simulated tube-reflector. (a) Conventional, focal distance of 14.1 mm. (b) Diverging beam scanning, virtual source distance, f_d = 10 mm. (b1) 29 transmissions, (b2) 95 transmissions, (b3) 157 transmissions with sub-aperture of 36 elements and f_d = 4.1 mm.

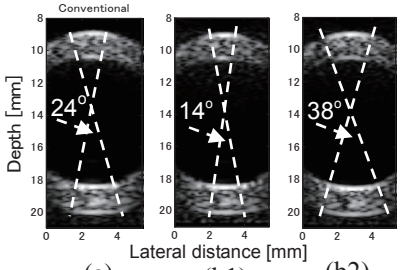

(a) (b1) (b2)

Fig. 5 Angular width of imaged region of the tube phantom for different numbers of transmissions. (a) Conventional linear scanning. (b) Diverging beam scanning, (b1) 29 transmissions, (b2) 95 transmissions.

5. Conclusion

Transverse cross-sectional image of cylindrical vessels could be obtained over wider regions than is possible with conventional linear scanning by employing multi-element diverging beams from a linear array transducer. It eliminates steering of transmit beams and the frame rate is still retained as in conventional linear scanning. This method is intended to be applied to *in vivo* transverse cross-sectional scanning of carotid arteries.

References

1. S. K. Jespersen, J. E. Wilhjelm, and H. H. Silleson: Ultras. Imag. **20** (1998) 81 - 102.
2. N. Nakagawa, H. Hasegawa, and H. Kanai: Jpn. J. Appl. Phys. **43** (2004) 3220 – 3226.
3. T. Mashiyama, H. Hasegawa, and H. Kanai: Jpn. J. Appl. Phys. **45** (2006) 4722 – 4726.
4. M. Karaman, P. Li, and M. O'Donell: IEEE Trans. UFFC **42** (1995) 429-442.
5. G. R. Lockwood, J. R. Talman, and S. S. Brunke: IEEE Trans. UFFC **45** (1998) 980-988.
6. S. I. Nikolov, K. Gammelmark, and J. A. Jensen: Proc. IEEE Ultras. Symp. **2** (1999) 1621-1625.
7. J. A. Jensen: Med. & Biol. Eng. Comp. 10th Nordic-Baltic Conf. Biomed. Imag. **4** Suppl. 1, Part 1 (1996) 351–353.